Results in Physics 26 (2021) 104344

Contents lists available at ScienceDirect

Results in Physics

journal homepage: www.elsevier.com/locate/rinp

An ultrathin and dual band metamaterial perfect absorber based on ZnSe for the polarization-independent in terahertz range

Yadgar I. Abdulkarim [a], Fatih Özkan Alkurt [c], Halgurd N. Awl [d], Fahmi F. Muhammadsharif [e], Mehmet Bakır [f], Sekip Dalgac [g], Muharrem Karaaslan [c], Heng Luo [b,*]

[a] Medical Physics Department, College of Medicals & Applied Science, Charmo University, 46023 Chamchamal, Sulaimania, Iraq
[b] School of Physics and Electronics, Central South University, Changsha, Hunan 410083, China
[c] Department of Electrical-Electronics Engineering, Iskenderun Technical University, 31200 Hatay, Turkey
[d] Department of Communication Engineering, Sulaimani Polytechnic University, Sulaimani 46001, Iraq
[e] Department of Physics, Faculty of Science and Health, Koya University, Koya 44023, Iraq
[f] Department of Computer Engineering, Bozok University, 66200 Yozgat, Turkey
[g] Department of Electric and Electronics Engineering, Sivas University of Science and Technology, 58050 Sivas, Turkey

ARTICLE INFO

Keywords:
Metamaterial
Dual band
Perfect absorber
Polarization independent absorber

ABSTRACT

In this work, a new metamaterial design is proposed to yield an ultra-thin and dual band metamaterials perfect absorber (MPA) to be operated in the frequency range from 15 to 35 THz. The proposed structure is consisted of a copper resonator deposited on a very thin Zinc Selenide ZnSe (0.6 μm) substrate, where the backside of the structure is covered with a metal plate to block the transmission of electromagnetic waves. Computer Simulation Technology (CST) was used to design and investigate the proposed structure. The absorption response of the proposed structure was found to be high enough with absorptivity of 98.44 and 99.28 at 22.46 THz and 28.95 THz, respectively. Results showed that the absorber is insensitive to the incident angle of 0°–60° in both transverse electric (TE) and transverse magnetic (TM) modes, respectively. The MPA was seen to be highly independent on the angles of polarization of the incident waves. The working mechanism of the proposed design was revealed by multiple reflection interference theory and a good agreement was confirmed between the calculated and simulated results. The proposed design can be used for possible applications of stealth technology and imaging.

Introduction

Metamaterials (MTMs) are artificially engineered materials whose present a unique feature of negative refraction against the electromagnetic waves [1–3]. Benefited by this property, research scientists have employed MTMs in the manipulation of electromagnetic waves for super lensing [4,5], invisibility cloaking [6,7], antennas [8,9], absorption in microwave [10,11] and terahertz region [12–16] as well as sensors in microwave and terahertz regions [17–23]. Moreover, because of the excellent characteristics of MTMs, they can be used in frequency selective absorption [24,25]. According to Kirchhoff's law of thermal radiation, the absorptivity of an object is equal to its thermal emissivity. Having enough information on emissivity of materials is important for the application of accurate measurement of non-contact temperature and for the calculations of heat transfer. Before determining the emissivity of the thermal emitter, its absorption properties are usually studied [26].

Researchers have proposed different approaches for controlling thermal emission of materials such as photonic crystals and dielectric structures [27,28]. However, with these materials one cannot control the permittivity, permeability, and sub-wavelength thickness precisely, whereas it is possible to tune the absorption response in MTMs for photovoltaics applications. For example, Rufanguar & Sabah designed and simulated a nanostructure-based MPA [29], followed by simplifying the design using symmetric structure for solar energy harvesting [30]. Luo et al. proposed a novel metamaterial absorber which is composed of a periodic array of dielectric cylinder sandwiched between nickel (Ni) films [31]. Li and Fan reviewed the recent developments of Nano

* Corresponding author.
E-mail addresses: yadgar.abdulkarim@charmouniversity.org (Y.I. Abdulkarim), fozkan.alkurt@iste.edu.tr (F. Özkan Alkurt), halgurd.awl@spu.edu.iq (H.N. Awl), mehmet.bakir@bozok.edu.tr (M. Bakır), muharrem.karaaslan@iste.edu.tr (M. Karaaslan), luohengcsu@csu.edu.cn (H. Luo).

https://doi.org/10.1016/j.rinp.2021.104344
Received 17 March 2021; Received in revised form 4 May 2021; Accepted 16 May 2021
Available online 21 May 2021

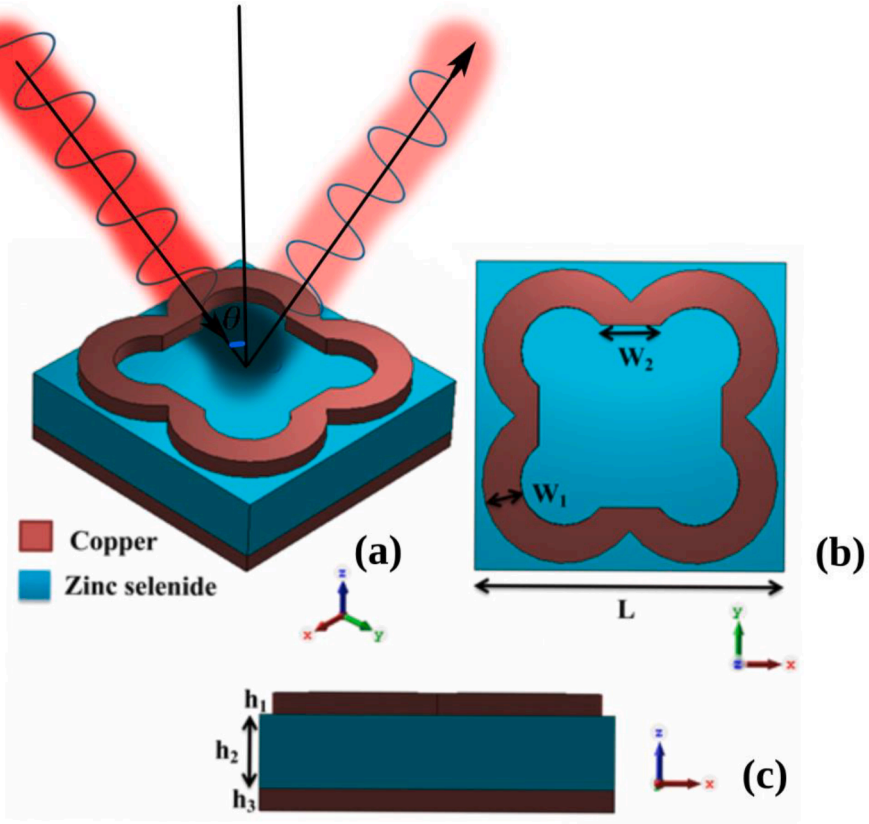

Fig. 1. (a) Perspective view, (b) top view and (c) side view of the dual-band metamaterials perfect absorber (MPA).

photonic control of thermal radiation, and highlighted some exciting energy application opportunities such as daytime radiative cooling, thermal textile, and thermos photovoltaic systems that are enabled by Nano photonic structures [32]. Wang et al. provided a conceptive design of self-adaptive photonic thermal management by tuneable radiative cooling and solar heating, and hence considering the absorption spectra of the atmospheric window range and solar energy [33]. Smith et al. designed and fabricated an absorptive metamaterial made of epsilon-near-zero indium tin oxide and silicon dioxide films for wideband perfect light absorption near the epsilon-near-zero wavelength [34]. Yongzhi Cheng et al. at Wuhan University of Science and Technology developed broadband tuneable terahertz metamaterials absorber based on different graphene resonators [35,36]. In the past years, researchers from different countries have shown their interest to work on terahertz range, thereby developing dual and multi-band metamaterials absorber using various structures [37–40].

The independency of the metamaterials-based devices on the angle of polarization is very important for practical applications including thermal and image sensing. Therefore, in this study, a new dual-band perfect metamaterial absorber is designed and proposed with polarization independent characteristic for possible application of thermal energy. Numerical results showed that the proposed design is insensitive to the angle of incident wave due to the presence of symmetrical resonator on the top of the structure. The suggested design is almost similar to clover leaf shape, offering two high absorption regions between 15 THz and 35 THz. This design is especially developed for easy production compared to those reported in literature [41–48]. Zinc selenide (ZnSe) presents several interesting properties such as low electrical resistivity, high direct band gap, high refractive index, broad band transparency, low optical absorption and high photosensitivity. These properties have made ZnSe to receive a considerable attention by researchers, leading to its application in solar cells, sensing and mid infrared sources [49–51]. In the current work, a simple clover leaf shaped resonator is printed on ZnSe/copper plate for IR perfect metamaterial absorbers. The parametric dimensions of the proposed deign were purposely tuned by using parametric study and genetic algorithm to simulate the perfect absorption in Terahertz frequency range. For practical applications, it is imperative to have a large-scale IR metamaterial absorber. The novelty of the proposed structure includes a simple design that provides perfect absorption response with independent-polarization angle in the mid-IR region. We believe that our proposed design can be potentially applicable in stealth technology, imaging and thermal energy harvesting.

Theory of the designed structure

In this work, full-wave finite integration technique (FIT) based on high-frequency electromagnetic solver, CST microwave studio was used to design the structure and simulate the results. Nowadays, CST makes it possible to use very difficult numerical calculations in the electromagnetic field through a number of software packages. Thus, MTM characteristics can be determined using a number of numerical calculations. During the simulation phase, very complex and long calculations can be easily performed, and the behaviours of large-scale and very different shapes of MTM structures, under the selected frequency range and selected boundary conditions, can be demonstrated. Scientists have had the opportunity to test electromagnetic materials in laboratory conditions under various boundary conditions. In numerical analysis, various boundary conditions have been used to analyse the structures such as PEC/PMC, PEC, free space, periodic and unit cell. In order to obtain the effective dimensions of the proposed structure and to simplify the simulation processes, unit cell was assigned for x-/y-directions and open add space was used for z-direction. It is important for an absorber that the resonator and free space can provide similar impedance by adjusting the parameters of the unit cell to decrease reflectivity, as shown in Fig. 1 (a). Fig. 1 shows the complete structure of the design with different pictorials. The proposed design consists of three main layers, including a

Table 1
The optimum parameters of the proposed design.

Parameter	L	h_1	h_2	h_3	W_1	W_2
Value	9.5 μm	30 nm	600 nm	30 nm	1.15 μm	1.825 μm

bottom copper ground plane with a thickness of 30 nm, ZnSe layer with a thickness of 600 nm and top MPA patterned copper with a thickness of 30 nm. ZnSe was added into the library of CST software by providing its permittivity and permeability parameters as 5.73 and 1, respectively [41]. The optimal values of the parameters shown in Table 1 were obtained by changing the dimensions and observing the performance of the proposed structure (see Fig. 1(b) and (c)). Thickness and dimensions of the proposed design were selected by using a built-in genetic algorithm in the CST software, in which the dielectric constant of the materials and the operating frequency range were utilized as inputs. The resonators were made up of copper with a conductivity of 5.96×10^7 S/m and thickness of 0.03 μm.

Results and discussion

Two resonant frequencies for the proposed MPA structure were clearly seen, as shown in Fig. 2. It is generally known that the primary requirement of an absorber is to confine the penetrated energy in the structure. To obtain a perfect absorber, the reflected and transmitted wave should be minimized to the smallest possible value (R (ω) &T (w) → 0). The absorptivity of the proposed structure can be calculated by: A (w) = 1-R (w)-T (w), where, A (w), $R(\omega)=|S_{11}|^2$ and $T(\omega)=|S_{21}|^2$ are the

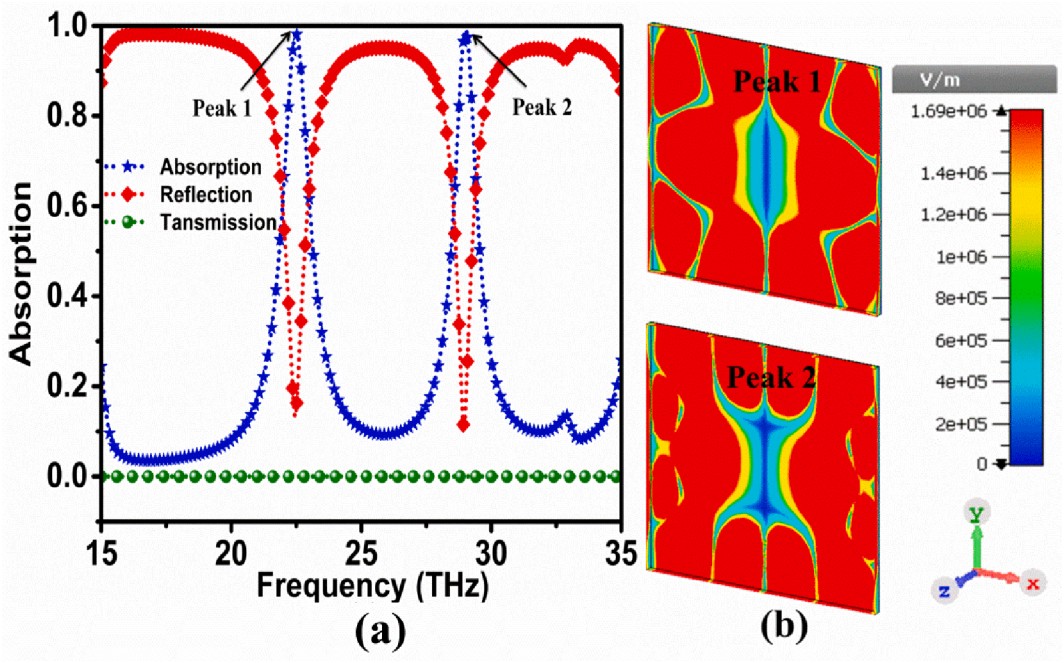

Fig. 2. (a) Simulated results of reflection, absorption and transmission spectra for the proposed dual-band MPA structure with optimized parameters and (b) Electric field distribution along Z-direction at resonant peak 1 and peak 2.

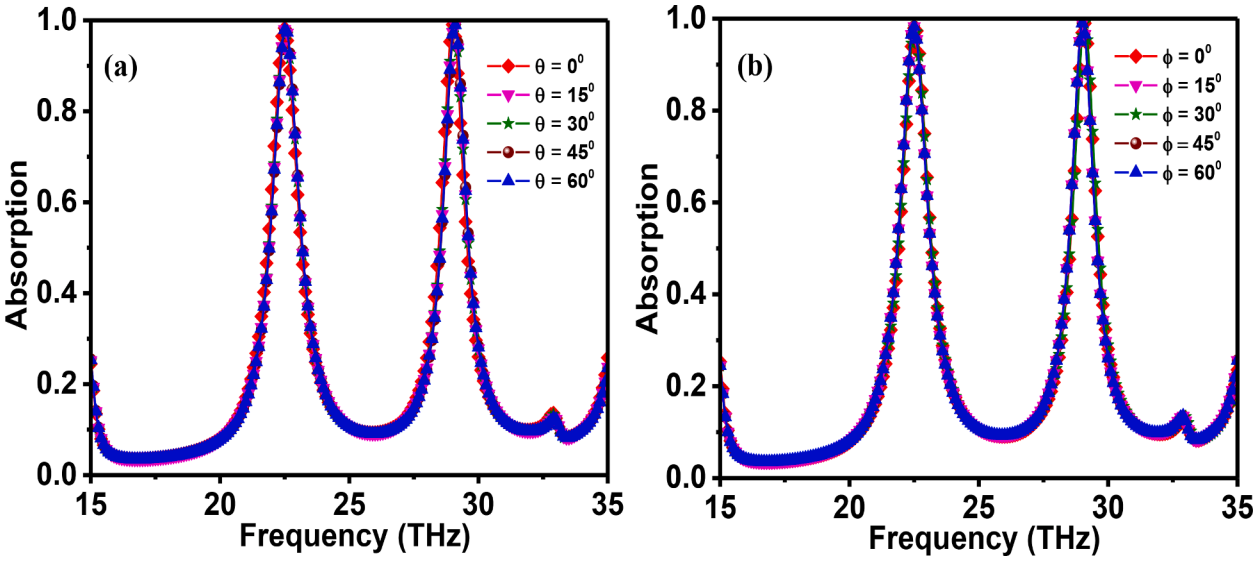

Fig. 3. (a) Absorption spectrum for the dual-band MPA at different incident angles and (b) the polarization independent of the structure from 0° to 60° for TM (or TE) modes.

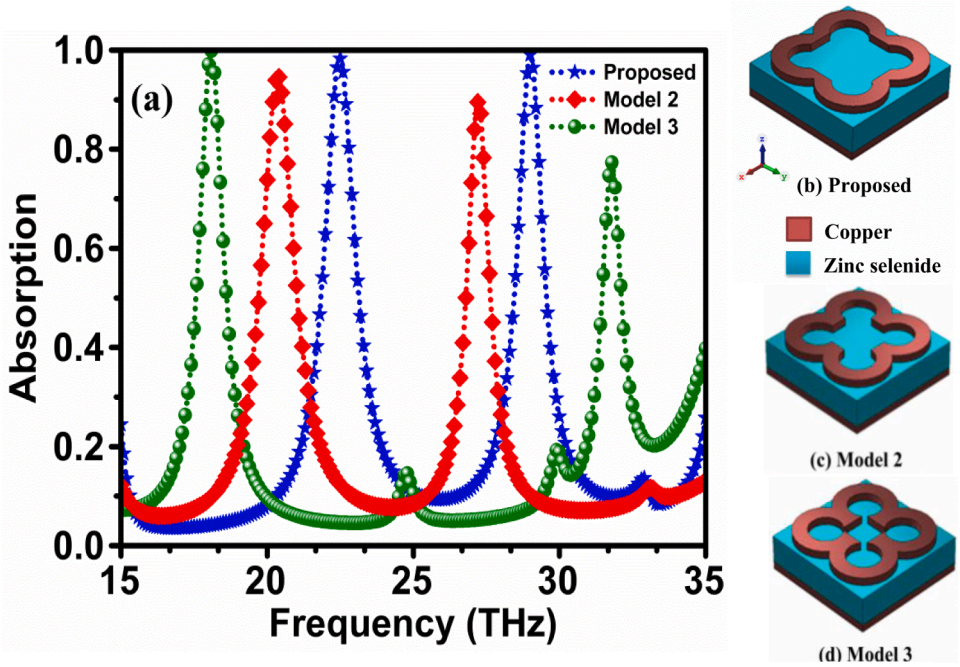

Fig. 4. (a) Absorption spectra of the three different structures shown as insets of (b), (c) and (d).

magnitude of the absorption which is related to the angular frequency, reflection and transmission corresponding to a certain frequency range, respectively. The backside of the designed structure was covered by a copper metal plate to minimize the transmission. Because the thickness of the copper film is much greater than the skin depth, the transmission would be close to zero ideally. Therefore, only the reflection value of the overall structure can be considered, which is directly related to the S_{11}. Hence, the absorption can be calculated as A (w) = 1-R (w). The metal backplate is a lossless conductor and hence its contribution is to reflect the transmission wave back to the dielectric part completely and hence achieving a perfect absorption by the ZnSe layer.

For better understanding the resonant absorption behaviour of the proposed dual band metamaterial absorber, electric field distributions for peak 1 and peak 2 were simulated, as shown in Fig. 2(b). It can be observed from the figure that maximum electric field distributions were mainly occurred around the resonator edges at resonant frequencies. Therefore, the resonator design plays an important role in defining the resonant frequencies and monitoring the electric field distributions induced by the electric field. The electric field component of incident wave excites free electrons causing a surface current, and the surface charge oscillates along the external electric field. This field causes magnetic dipole moment, and it is this dipole moment that results in resonant absorption. This indicates that the electric field of the incident electromagnetic wave is coupled with the upper and lower part of the resonator and hence resonates along with the electric field direction, which can be interpreted by a simple dipole–dipole interaction [52,53].

We characterized the polarization dependent of absorption for the proposed structure under normal incidence of TE waves, as shown in Fig. 3(a). Moreover, we considered the absorption spectrum at five different polarization angles from 0° to 60°, taking into consideration the rotational symmetry of the unit cell structure. It is clear from the figures that the proposed structure maintained excellent absorption stability under different polarization angles. Also, the absorption performance at higher frequencies was found to be stable under different polarization angles. The absorber provides the same result in response to different polarization of incidence waves. This is achieved by utilizing a symmetric resonator. When the incidence wave hits the symmetric resonator at different phi angle, the resonator behaves similarly and provides the same response. This is considered as the basic mechanism of polarization independent for the symmetric structures. The performance of the perfect metamaterial absorber over different incident angles of electromagnetic radiations revealed that the proposed design can be a good candidate for the application of terahertz and microwave bands. Hence, perfect metamaterials absorbers have to maintain an outstanding absorption response in different incident angles. One can see from Fig. 3(b) that the absorption spectrum of the metamaterials structure simulation remained unchanged at different incident angles, suggesting its insensitivity to the incident angles of electromagnetic waves and hence confirming a high symmetry of the structure.

In addition to the proposed absorber model, we developed two different models with the aim of further understanding the absorption features of the structures and to define a design with polarization independent, as shown in Fig. 4. The extended models were established based on the concept of increasing the circumference of the attached semi-circular resonators followed by recording their absorption properties. As such, the semicircles in model 2 were fixed at three quarters of a complete circle, while in model 3 the circumferences of the semicircles were further increased. In order to verify the numerical results of the proposed MPA, the three different models were investigated in the frequency range from 15 to 35 THz, as shown in Fig. 4(a). It is obvious from the figure that the designed models have dual resonant frequencies with capability of absorbing 99% of the energy propagating through their medium at frequencies of 22.46 THz and 28.95 THz. Noticeably, the absorption activity in model 2 has reached 95% and 90% at 21 THz and 27 THz, respectively, which are yet lower than the absorption response that was achieved by the proposed model. When it comes to model 3, the absorption peak at its lowest resonant frequency of 17 THz was found to be 99.9%, which is the highest one among the absorption peaks of other structures. However, model 3 presented worst absorption of 80% at 33 THz compared to those of the proposed model and model 2. Concludingly, the proposed model was a better absorber amid the investigated models.

Moreover, we investigated the polarization and polarization angle dependency of absorption in the two models. The incident waves were set as TE and TM polarization, while polarization angle was chosen to be theta = 0 and theta = 90° for each polarization type. From Fig. 5(a) and (b), one can see that the polarization angle is one of the main parameters affecting the absorption response in such MTM based resonators. In case

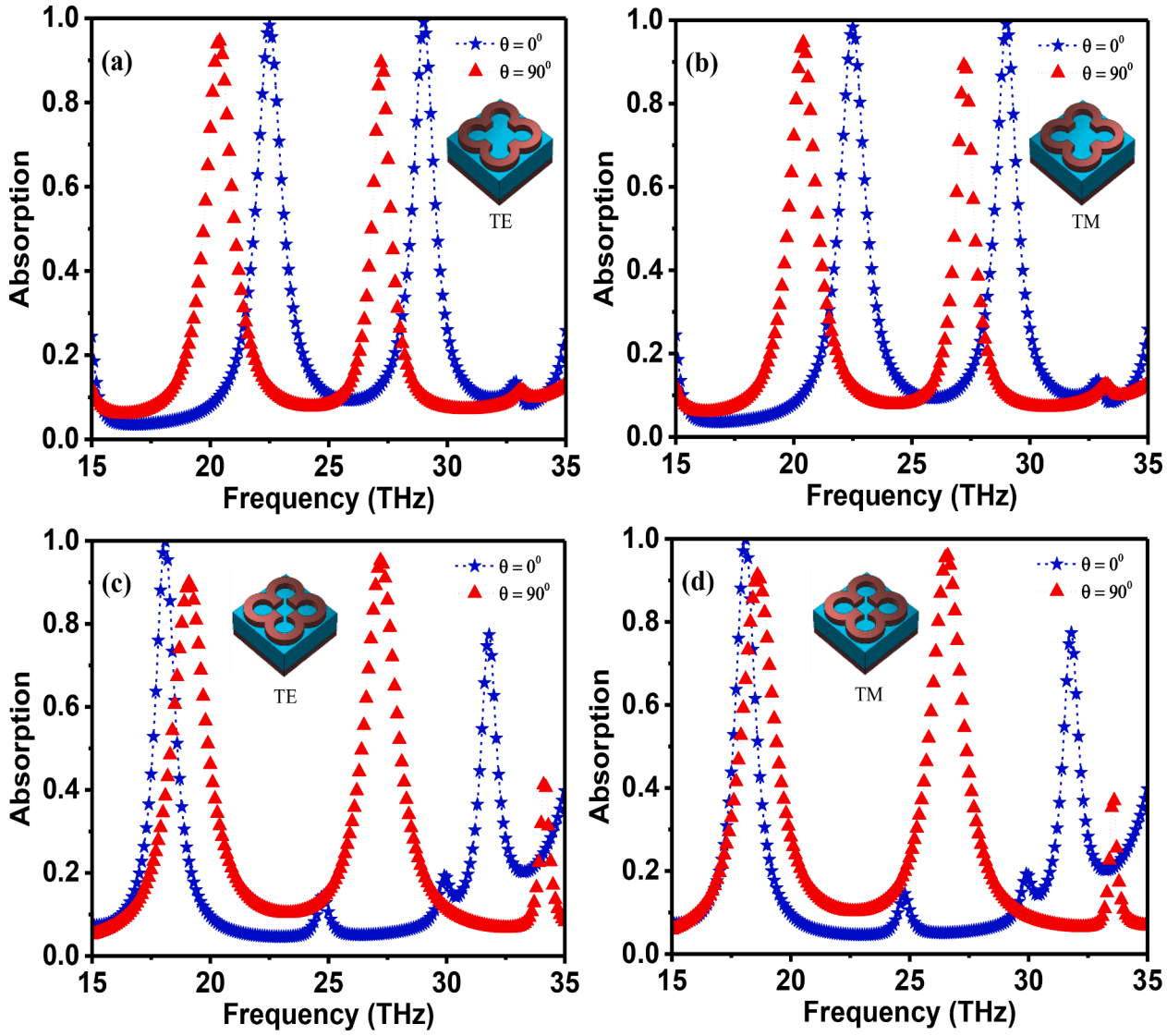

Fig. 5. (a) and (b) show absorption results with the maximum and minimum operating angle for model 2 in TE and TM modes, respectively, while (c) and (d) show the absorption spectrum for model 3 under TE and TM, respectively.

of employing TE polarization mode, when the polarization angle was set to theta = 0 and theta = 90°, a multi band absorption property was achieved. Results showed that the position of the absorption peaks is changed with the change of incident angle. For instance, the resonant frequencies were appeared at 23 THz and 27 THz for 0° and at 19 THz and 24 THz for 90°, as shown in Fig. 5(a). Fig. 5(b) shows the response of model 2 when a TM polarization wave was applied instead of TE polarization. It was observed that the resonant frequencies remained unchanged, meaning that the structure of model 2 is polarization independent. It is worth to mention that the absorption rate at theta = 0° is higher than that at theta = 90° for both TE and TM polarization modes. Also, the same procedure was applied to model 3 in order to observe the polarization and polarization angle dependency on the absorption response. In case of TE mode and angle 0°, the absorption by model 2 was found to reach a maximum value of 99.9% at 17 THz. However, this was only 80% at 33 THz resonant frequency. When we set theta = 90°, similar absorption activity was observed at 18 THz and 27.5 THz. Also, TM polarization wave was applied to model 3 in the same condition as of model 2 and it was noticed from the results that model 3 is polarization independent.

Fig. 6 shows the effect of resonator type, substrate type and resonator thickness on the absorption of the proposed structure. It was seen from the results of using different types of resonators, namely aluminum, copper, gold and iron, that for each resonator there will be a strong dual-band absorption at 22.46 THz and 28.95 THz, as shown in Fig. 6(a). Moreover, the effect of Arlon AD 410, ZnSe, FR4 and Rogers RT 5870 substrates on the absorption property was considered, as shown in Fig. 6 (b). For ZnSe material, the absorption rate has reached a maximum of 99.9% at 22.46 THz and 28.95 THz. Also, FR4 and Arlon AD 410 has led to producing a reasonably high absorption peak at 26 THz and 27 THz, respectively. However, Rogers RT 5870 resulted in a minimum absorption rate of 85% at 33 THz compared to the other substrates. Finally, the impact resonator (*w1*) thickness on the absorption was analyzed by adjusting the thickness to different values. As shown in Fig. 6(c), a dual-band absorption behavior was achieved at 22.46 THz and 28.95 THz for a wide range of thickness. It is seen from the figure that 99% of the energy is absorbed by the structure at varied thickness. It can be said that the thickness variation did not show a pronounced effect on the absorption properties of the proposed structure.

The mechanism of the absorption by the proposed dual-band MPA was interpreted based on interference theory. Our metamaterial structure can be modeled by a Fabry-Pérot-like resonance cavity, which has a multiple interferences effect in multi reflection for the incident electromagnetic waves. In the designed structure, a strong local electro-

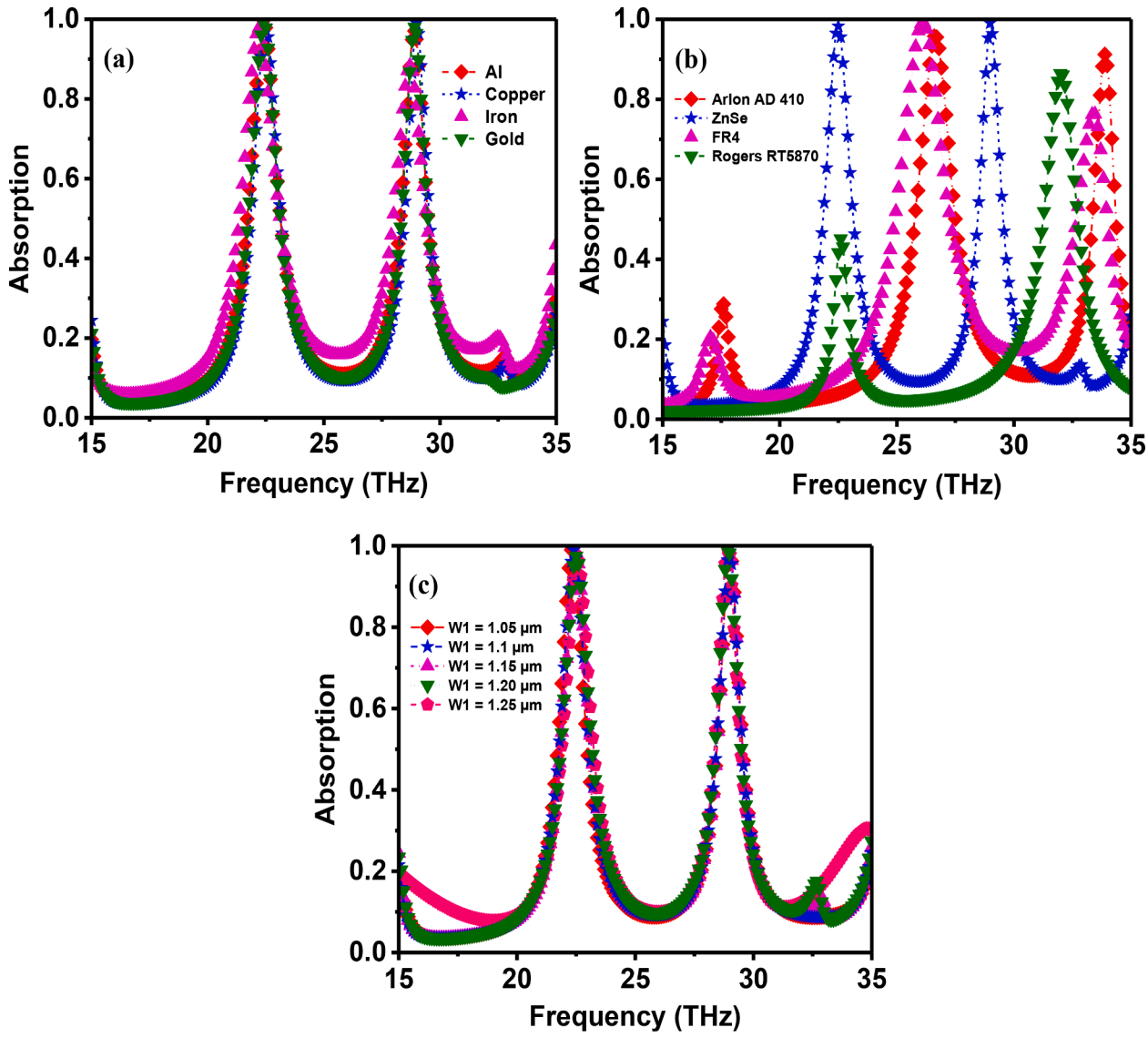

Fig. 6. The influence of (a) resonator type, (b) substrate type and (c) resonator thickness on the absorption response of the proposed dual-band MPA.

magnetic resonance and impedance matching has occurred between the MPA and free space, resulting in the generation of two highly absorptive peaks. The interference taken place between the direct reflections from air–spacer with clover leaf shaped resonator has led to the overlapping of multiple reflections [54]. Fig. 7(a) shows the working mechanism of the model by the analysis of absorption for the dual-band metamaterials absorber based on interference theory. As it can be seen from the figure, the multiple reflection interference model of the dual-band MPA, consisting of two interfaces from the top clover leaf shaped simple resonator and the bottom of the structure covered by the ground plane, are considered as a two non-thickness surface. This interference model can be defined by an uncoupled system, in which the near-field coupling between resonator layer and copper layer can be neglected. The clover leaf resonator works as a surface which can partially transmit/reflect the incident electromagnetic waves. Later on, this part of the incident waves are transmitted and passed through the ZnSe substrate (spacer) until they are reached the copper ground plate which has a complex phase propagation of $\beta = -\sqrt{\varepsilon_r}K_o t_s$, where ε_r is the dielectric constant of the substrate,K_o is denoted free space wave number and t_s is the thickness of the substrate. When the incident wave hits the proposed structure at the top layer (clover leaf resonator) and at the air- spacer interface, partial of the incident wave is reflected back to air, having a reflection coefficient of $\vec{r_{12}} = r_{12}.e^{\varnothing_{12}}$. The other parts of the incident wave are transmitted into the spacer with a transmission coefficient of $\vec{t_{12}} = t_{12}.e^{\varnothing_{12}}$. The rest of the incident wave continues to propagate until it arrives the copper metal at the bottom layer. The reflection at the ground plate (layer) equals to minus 1 (r_{23} = -1), while some of the incident waves are reflected and transmitted again at the air-spacer interface, which are denoted by $\vec{r_{21}} = r_{21}.e^{\varnothing_{21}}$ and $\vec{t_{21}} = t_{21}.e^{\varnothing_{21}}$. Fig. 7(a) shows the multi reflection process from air –spacer- ground plane. It is concluded that the overall reflection is the sum of the all multiple reflections mentioned above. The total reflection coefficient of the proposed structure can be numerically calculated by using this equation [53]:

$$r = \vec{r_{12}} - \frac{t_{12}.t_{21}.e^{i2\beta}}{1 + r_{21}.e^{i2\beta}}$$

The reflection of the proposed structure can be theoretically obtained by using equation (1), followed by absorption determination using the equation: $A = 1 - |r|^2$, that is to obtain the multi reflection at air –spacer interface, as shown in Fig. 7(a). The copper plate at the bottom of the proposed design was first removed then the numerical simulation was achieved to find the unknown parameters in equation (1). The magnitude and the phase (degree) of the transmission and reflection at the air

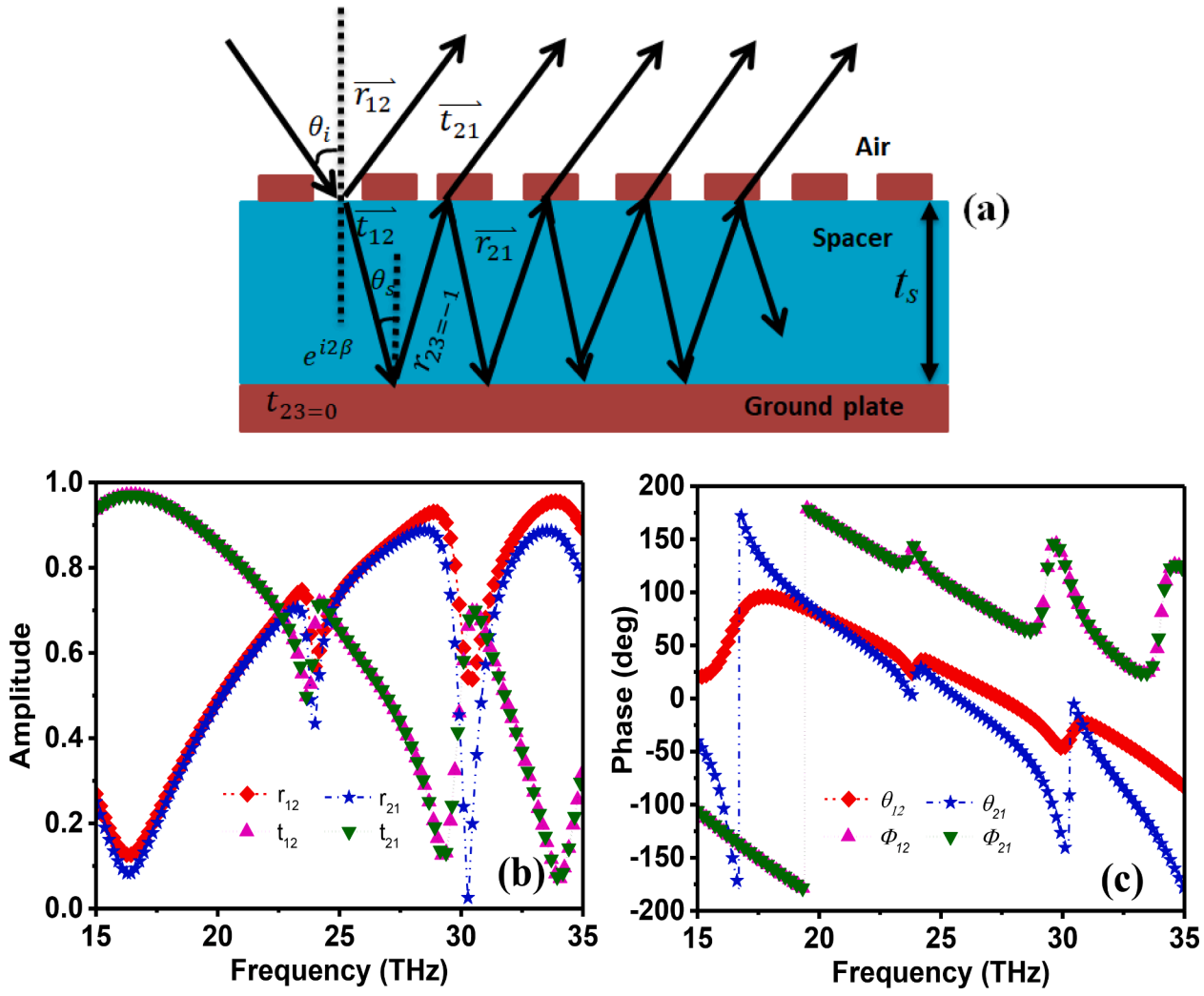

Fig. 7. (a) Interference model for the dual-band MPA structure shows the multiple reflections based on Fabry-Pérot interference theory, (b) and (c) shows the numerical results of the magnitude and phase (degree) of the complex reflection and transmission coefficient at air spacer interface, respectively.

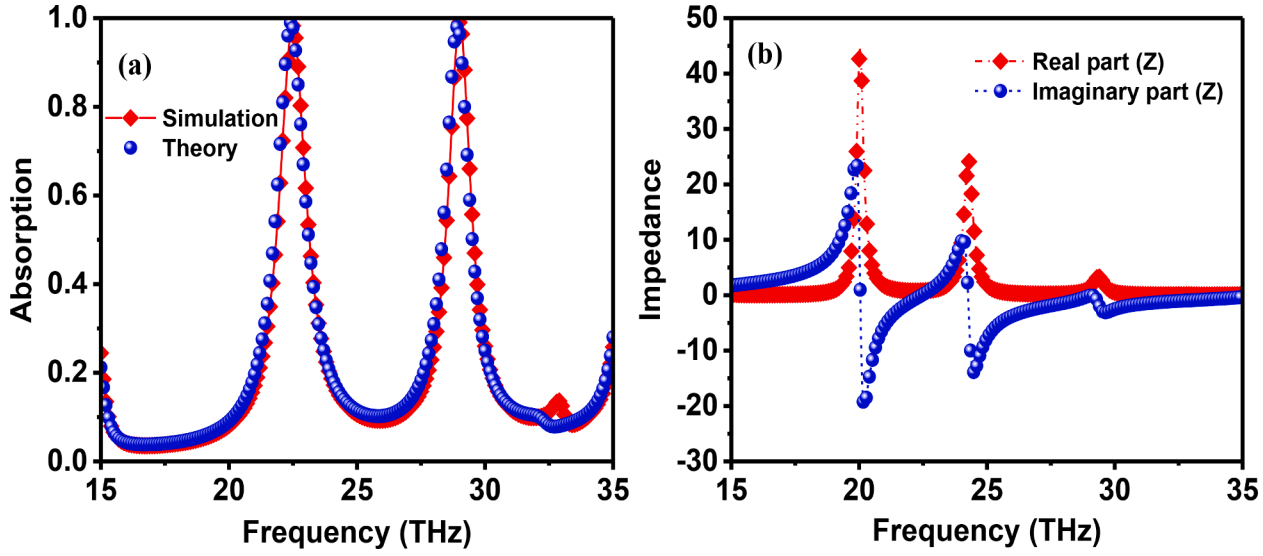

Fig. 8. (a) Comparison of the simulated (red line) and calculated (blue line) absorption results and (b) real and imaginary part of the impedance for the proposed designed structure. (For interpretation of the references to colour in this figure legend, the reader is referred to the web version of this article.)

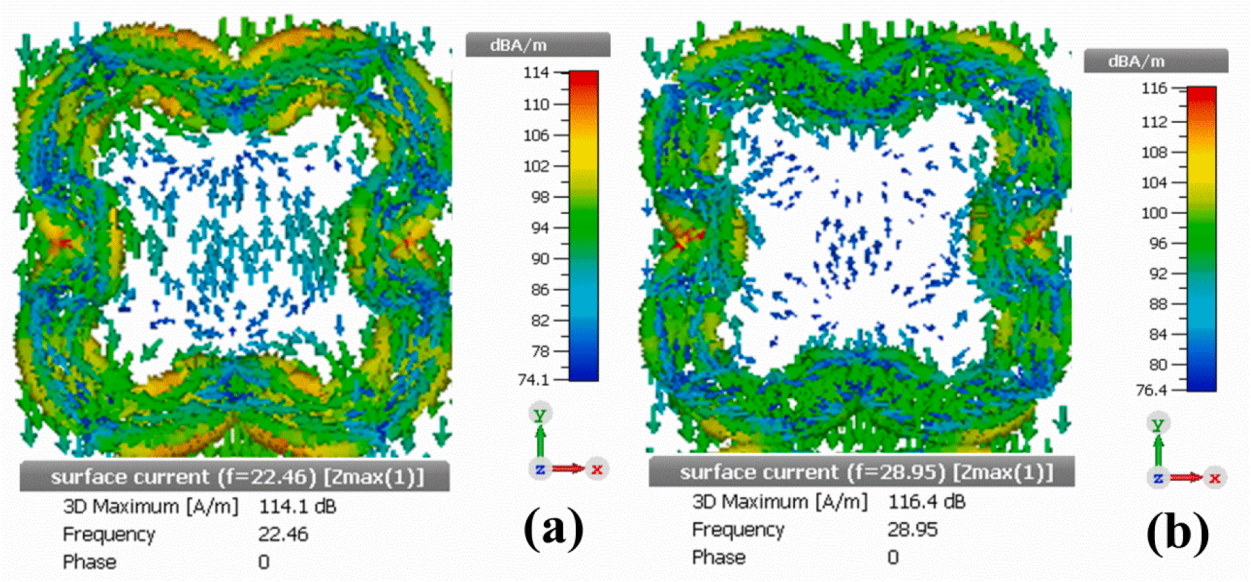

Fig. 9. Simulated surface current distribution at (a) 22.46 THz and (b) 28.95 THz for the dual band MPA.

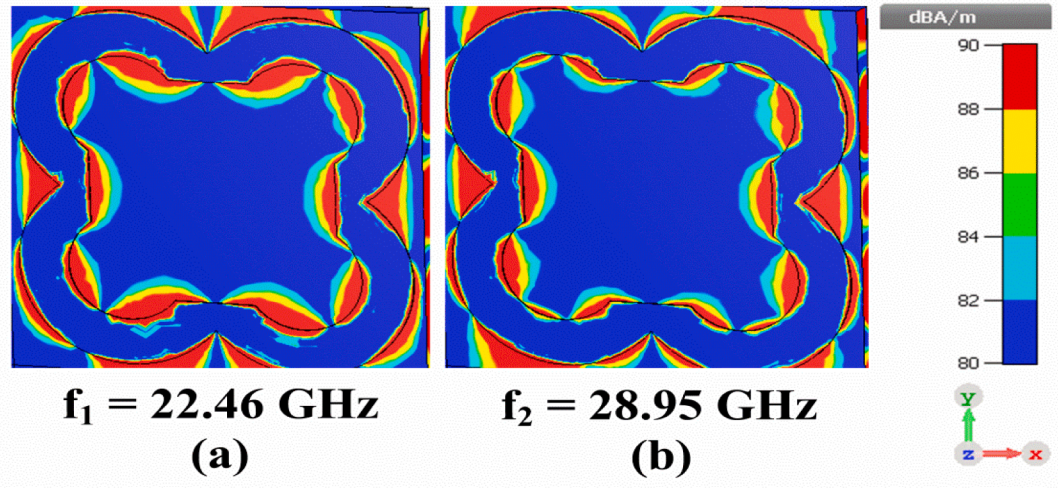

Fig. 10. Magnetic field distribution at two different resonance peaks (a) 22.46 THz and (b) 28.95 THz for the dual band MPA.

Table 2
Comparison of the results of this work with those reported in literature.

Ref.	Technique used	Operating frequency (THz)	Unit cell dimension (μm^2)	Substrate Thicknes (μm)	Absorptivity	Peak numbers
[12]	Multiple metallic resonators	2–5	36 × 36	2	97–100	Dual
[13]	Cross metal array resonator	12–28	4 × 4	1.5	99	Single
[14]	Two nested metallic circular ring resonators	0–4.5	80 × 80	18	99.83–98.92–99.96–99.35 and 99	Five
[15]	Gold resonator	4–8	43.8 × 43.8	8.1	99.3–99.2–99.4–98.1–95.2	Five
[16]	Periodic cross-shaped grooves	0–3.5	50 × 50	45	97.80–95.8	Dual
[22]	Pattern asymmetric metallic cross	0–3.4	80 × 80	11	99.07–99.84–99.01	Triple
[23]	Metallic Strip Resonator	1–3.25	90 × 90	10	98–99	Dual
[43]	FOUR-fold meander wire	1–3	55 × 50	15	93–100	Dual
[44]	Au Reflector	2–8	30 × 35	5	99–99	Dual
[45]	SPLIT ring dish resonator	1.925–6.3	24 × 24	1.2	100–99-100	Single Dual
[46]	Au rectangular strips	0–4.05	60 × 60	2	−99–100–100	Triple
[47]	graphene based meshed square patch FSS	0–4	42 × 42	22	99–97	Dual
[48]	Thin graphene-patterned array	1–7	3 × 3	10	99–98-99–99	Quad
This Work	Single metallic resonator	15–35	9.5 × 9.5	0.6	98.44–99.28	Dual

Table 3
Comparison of the current work with those reported in literature in terms of structure layer, central frequency, absorption percentage, TE, TM polarization, and angle of incident.

Ref.	Structure	Central frequency	Absorption	Polarization	Angles	Year published
[12]	Al/TiO2/Al	3.5	>90%	TE and TM	0–90	2020
[13]	Metal layer/Dielectric layer/Metal layer	20	>90%	–	0–50	2020
[14]	Copper/Polyimid/Silicon	2.25	>90%	–	0–90	2018
[15]	Au/Graphene/SiO2/Au	5.51	>90%	TE and TM	0–90	2020
[16]	Gold/SiO2/Graphene/SiO2	0.94	>90%	–	–	2019
[22]	Au/dielectric layer/Au	1.7	>90%	–	–	2016
[23]	Au/dielectric slab/Au	2.25	>90%	–	0 and 90	2015
[43]	Gold/PDMS/Gold	2	>90%	TE and TM	0–90	2018
[44]	Au/SiO2/Au	5	>90%	–	–	2019
[45]	Gold/SiO2/Gold	4.375	>90%	TE	0–60	2018
[46]	Au/dielectric slab/Au	2.25	>90%	–	–	2019
[47]	Graphene FSS/polyimide layer/perfect electric conductor (PEC)	2	>90%	TE	0–60	2020
[48]	Graphene/SiO2/Gold	4	>90%	TE	0–45	2021
This Work	Copper/ZnSe/copper	25 THz	>90%	TE and TM	0–60	2021

–space interface was numerically achieved and the curves are illustrated in Fig. 7(b) and (c).

Fig. 8 shows the absorption and impedance spectra of the proposed MPA. One can observe that there exist two main perfect absorption peaks at around 22.46 and 28.95 THz resonant frequency. It was found that the simulated and calculated absorption spectra are well matched, confirming sufficient reproducibility of the achieved results in the frequency range of investigation from 15 to 3 THz. Noteworthy, the dual band MPA nature of the proposed design with negative impedance has been clearly detected at the two characteristic resonant frequencies. The values of real impedance at the resonant peaks were found to reach 45 and 6 Ω, respectively.

Fig. 9 shows the surface current distribution which is generated due to the incident electromagnetic interaction with the MPA at the two resonant frequencies of 22.46 and 28.95 THz. It was noticed that the surface current density at the lower resonant frequency is mostly concentrated across the edges of the clover leaf-shaped layer and at the center of ZnSe layer. However, the increased resonant frequency has led to decreased surface current density across the ZnSe layer with less pronounced decrease at the edges of clover leaf-shaped layer.

Fig. 10 shows the magnetic field distribution of the incident electromagnetic across the surface of the MTM absorber at the dual resonant frequencies of 22.46 and 28.95 THz. One can see that lowest magnetic field has distributed on the core of the patterned copper layer and on the center of ZnSe layer. This can be ascribed to the non-magnetic nature of the copper and ZnSe compound. Nevertheless, the density of magnetic field is highest at the boundaries of the copper and ZnSe interfaces, which might be attributed to the presence of some kinds of interface interaction between the copper metal and ZnSe, thereby yielding a paramagnetic responsive structure.

The results obtained in this work were compared with those reported in other research papers, as shown in Tables 2 and 3. The comparison has been made in terms of the technique used on the top of the substrate, operation frequency range, unit cell dimensions, substrate thickness, absorptivity and peaks number. As shown in Table 1, the proposed structure has a smaller unit cell of $9.5 \times 9.5\ \mu m^2$ compared to that of other similar works and that the substrate thickness used in our design is $0.6\ \mu m$. Hence, in addition to the reduction in device profile, the absorptivity was maintained quite high and independent on the polarization angle for each of TE and TM waves compared to those of other devices reported in literature.

Conclusions

In summary, an ultra-thin and dual-band metamaterial perfect absorber was successfully presented in the wide frequency range from 15 to 35 THz. The proposed design showed two resonant peaks of nearly perfect absorptivity of 99.28% and 98.44% at the frequency of 22.46 THz and 28.95 THz, respectively. The proposed design remained insensitive and independent to the change of incident angle from 0° to 60° and polarization angle for both TE and TM, respectively. The theoretical calculation of the absorption was found to be almost the same as the numerical results, showing that the proposed design is symmetric with highly favourable performance. Furthermore, the simulation study of the surface current and magnetic field distribution revealed the absorption mechanism inside the MPA structure. The results of this work were seen to be better compared with those of similar published papers in literature. The results were compared in terms of unit cell dimension, thickness of the substrate, frequency range, absorptivity, polarization angle and used techniques. We believe that our proposed dual-band MPA can be potentially used for different applications such as stealth, imaging, sensing.

Funding

This research was funding by the National Natural Science Foundation of China (Grant No. 51802352), Central South University (Grant No. 2018zzts355) and Teaching reform for postgraduate students of Central South University (Grant No. 2019JG085).

Data availability statement

No new data were created or analysed in this study. Data sharing is not applicable to this article.

Author contributions statement

We would like to submit the enclosed manuscript entitled “An Ultrathin and Dual Band Perfect Metamaterial Absorber Based on ZnSe for the Polarization-Independent Applications in Terahertz Range”, which we wish to be considered for publication in “Results in Physics” All all co-authors are contributed this work as bellow: Yadgar I. Abdulkarim and Muharrem Karaaslan conceived the idea; Yadgar I. Abdulkarim and Halgurd N.Awl performed the simulations; Yadgar I. Abdulkarim1, Fatih Özkan Alkurt and Mehmet Bakır wrote the manuscript; Fahmi F. Muhammadsharif, Sekip Dalgac and Muharrem Karaaslan revised the manuscript; H.L revised the manuscript and supervises this work. I would like to declare on behalf of my co-authors that the work described was original research that has not been published previously, and not under consideration for publication elsewhere, in whole or in part. All the authors listed have approved the manuscript that is enclosed.

Declaration of Competing Interest

The authors declare that they have no known competing financial interests or personal relationships that could have appeared to influence

the work reported in this paper.

References

[1] Abdulkarim YI, Deng L, Yang J-L, Çolak Ş, Karaaslan M, Huang S-X, He L-H, Luo H. Tunable left-hand characteristics in multi-nested square-split-ring enabled metamaterials. J Central South Univers 2020;27(4):1235–46. https://doi.org/10.1007/s11771-020-4363-5.

[2] 2. Saadeldin AS, Hameed MFO, Elkaramany EMA, Obayya SSA. Highly sensitive terahertz metamaterial sensor. IEEE Sensors Journal, 19(18),. IEEE Sensors 2019; 19(18): 7993-9. 10.1109/JSEN.2019.2918214.

[3] Abdulkarim YI, Deng L, Karaaslan M, Altıntaş O, Awl HN, Muhammadsharif FF, et al. Novel metamaterials-based hypersensitized liquid sensor integrating omega-shaped resonator with microstrip transmission line. Sensors 2020;20(3):943. https://doi.org/10.3390/s20030943.

[4] M. MMS, C. S. Dual-metasurface superlens: A comprehensive study. Physical Review B. 2019;100(20):205426. 10.1103/PhysRevB.100.205426.

[5] Yuan G, Rogers KS, Rogers ETF, Zheludev NI. Far-field superoscillatory metamaterial superlens. Phys Rev Appl 2019;11(6). https://doi.org/10.1103/PhysRevApplied.11.064016.

[6] Ma F, Xu Y, Wu JH. Shell-type acoustic metasurface and arc-shape carpet cloak. Sci Rep 2019;9(1):8076. https://doi.org/10.1038/s41598-019-44619-z.

[7] Zou S, Xu Y, Zatianina R, Li C, Liang X, Zhu L, et al. Broadband Waveguide cloak for water waves. Phys Rev Lett 2019;123(7). https://doi.org/10.1103/PhysRevLett.123.074501.

[8] Imani MF, Gollub JN, Yurduseven O, Diebold AV, Boyarsky M, Fromenteze T, et al. Review of metasurface antennas for computational microwave imaging. IEEE Trans Antennas Propag 2020;68(3):1860–75. https://doi.org/10.1109/TAP.2020.2968795.

[53] Abdulkarim YI, Awl HN, Muhammadsharif FF, Karaaslan M, Mahmud RH, Hasan SO, et al. A Low-Profile Antenna Based on Single-Layer Metasurface for Ku-Band Applications. International Journal of Antennas and Propagation. 2020; 2020 8813951. 10.1155/2020/8813951.

[9] Wanga Y, Chen Z, Xu D, Yi Z, Chen X, Chen J, et al. Triple-band perfect metamaterial absorber with good operating angle polarization tolerance based on split ring arrays. Results Phys 2020;16. https://doi.org/10.1016/j.rinp.2020.102951.

[10] I.Abdulkarim Y, Deng L, Altıntaş O, Ünal E, Karaaslan M. Metamaterial absorber sensor design by incorporating swastika shaped resonator to determination of the liquid chemicals depending on electrical characteristics. Physica E: Low-dimensional Systems and Nanostructures. 2019;114:113593. 10.1016/j.physe.2019.113593.

[11] Daniel S, Bawuah P. Right-angle shaped elements as dual-band metamaterial absorber in terahertz. Photonic Sensor 2019;10:233–41. https://doi.org/10.1007/s13320-019-0573-6.

[12] " MZ. Design and measurement of a narrow band metamaterial absorber in terahertz range. Optical Materials 2020;100 109712. 10.1016/j.optmat.2020.109712.

[13] Meng T, Hu D, Zhu Q. Design of a five-band terahertz perfect metamaterial absorber using two resonators. Opt Commun 2018;415:151–5. https://doi.org/10.1016/j.optcom.2018.01.048.

[14] Jain P, Bansal S, Prakash K, Sardana N, Gupta N, Kumar S, et al. Graphene–based tunable multi–band metamaterial polarization–insensitive absorber for terahertz applications. J Mater Sci: Mater Electron 2020;31:11878–86. https://doi.org/10.1007/s10854-020-03742-8.

[15] Qi Limei, Liu Chang, Shah Syed Mohsin Ali. A broad dual-band switchable graphene-based terahertz metamaterial absorber. Carbon 2019;153:179–88. https://doi.org/10.1016/j.carbon.2019.07.011.

[16] Abdulkarim YI, Muhammadsharif FF, Bakır M, Awl HN, Karaaslan M, Deng L, Huang S. Hypersensitized metamaterials based on a corona-shaped resonator for efficient detection of glucose. Appl Sci 2021;11:103. https://doi.org/10.3390/app11010103.

[17] Abdulkarim Y. I., L. Deng, H. Luo, S. Huang, M. Karaaslan, O. Altıntaş, M. Bakır, F. F. Muhammadsharif, H. N.Awl, C. Sabah and K. S. L. Al-badri. Design and study of a metamaterial based sensor for the application of liquid chemicals detection. Journal of Materials Research and Technology, 2020, 9(5): 10291-10304, 10.1016/j.jmrt.2020.07.034.

[18] Chen Fu, Chen Youngzhi, Luo Hui. Temperature tunable narrow-band terahertz metasurface absorber based on InSb micro-cylinder arrays for enhanced sensing application. IEEE Access 2020;8:82981–8. https://doi.org/10.1109/ACCESS.2020.2991331.

[19] Abdulkarim YI, Deng L, Muhrram K, Eunal U. Determination of the liquid chemicals depending on the electrical characteristics by using metamaterial absorber based sensor. Chem Phys Lett 2019;732. https://doi.org/10.1016/j.cplett.2019.136655. 136655.

[20] Zou Haijun, Cheng Yongzhi. A thermally tunable terahertz three-dimensional perfect metamaterial absorber for temperature sensing application. Mod Phys Lett B 2020;34(18):2050207. https://doi.org/10.1142/S0217984920502073.

[21] Wang Ben-Xin, Wang Gui-Zhen, Sang Tian. Simple design of novel triple-band terahertz metamaterial absorber for sensing application. J Phys D Appl Phys 2016;49. https://doi.org/10.1088/0022-3727/49/16/165307.

[22] Wang B-X, Zhai X, Wang G-Z, Huang W-Q, Wang LL. A novel dual-band terahertz metamaterial absorber for a sensor application. Journal of Applied Physics 2015;117:014504 10.1063/1.4905261.

[23] Xu C, Qu S, Pang Y, Wang J, Yan M, Zhang J, et al. Metamaterial absorber for frequency selective thermal radiation. Infrared Phys Technol 2018;88:133–8. https://doi.org/10.1016/j.infrared.2017.08.017.

[24] He Y, Wu Q, Yan S. Multi-band terahertz absorber at 0.1–1 THz frequency based on ultra-thin metamaterial. Plasmonics 2019;14:1303–10. https://doi.org/10.1007/s11468-019-00936-7.

[25] 26. Du K-K, Li Q, Lyu Y-B, Ding J-C, Lu Y, Cheng Z-Y, et al. Control over emissivity of zero-static-power thermal emitters based on phase-changing material GST. Light: Science & Applications 2017;6:e16194. 10.1038/lsa.2016.194.

[26] Ito K, Watari T, Nishikawa K, Yoshimoto H, Iizuka H. Inverting the thermal radiative contrast of vanadium dioxide by metasurfaces based on localized gap-plasmons. APL Photon 2018;3(8). https://doi.org/10.1063/1.5025947.

[54] Zhang X, Zhang Z-G, Wang Q, Zhu S-N, Liu H. Controlling thermal emission by parity-symmetric fano resonance of optical absorbers in metasurfaces. ACS Photon 2019;6(11):2671–6. https://doi.org/10.1021/acsphotonics.9b00024.

[27] Rufangura P, Sabah C. Dual-band perfect metamaterial absorber for solar cell applications. Vacuum 2015;120(8):68–74. https://doi.org/10.1016/j.vacuum.2015.05.033.

[28] Rufangura P, Sabah C. Design and characterization of a dual-band perfect metamaterial absorber for solar cell applications. J Alloy Compd 2016;671:43–50. https://doi.org/10.1016/j.jallcom.2016.02.066.

[29] Luo M, Shen S, Zhou L, Wu S, Zhou Y, Chen L. Broadband, wide-angle, and polarization-independent metamaterial absorber for the visible regime. Opt Express 2017;25(14):16715–24. https://doi.org/10.1364/OE.25.016715.

[30] Li W, Fan S. Nanophotonic control of thermal radiation for energy applications. Opt Express 2018;26(12):15995–6021. https://doi.org/10.1364/OE.26.015995.

[31] Wang W, Zhao Z, Zou Q, Hong B, Zhang W, Wang GP. Self-adaptive radiative cooling and solar heating based on a compound metasurface. J Mater Chem C 2020;8(9):3192–9. https://doi.org/10.1039/C9TC05634C.

[32] Smith EM, Chen J, Hendrickson JR, Cleary JW, Dass C, Reed AN, et al. Epsilon-near-zero thin-film metamaterials for wideband near-perfect light absorption. Opti Mater Express 2020;10(10):2439–46. https://doi.org/10.1364/OME.404169.

[33] Cheng Yongzhi, Zhao Haolin, Li Chan. Broadband tunable terahertz metasurface absorber based on complementary-wheel-shaped graphene. Opt Mater 2020;109. https://doi.org/10.1016/j.optmat.2020.110369.

[34] Chen Fu, Cheng Yongzhi, Luo Hui. A broadband tunable terahertz metamaterial absorber based on single-layer complementary gammadion-shaped graphene. Materials 2020;13(4):860. https://doi.org/10.3390/ma13040860.

[35] Li Wangyang, Cheng Yongzhi. Dual-band tunable terahertz perfect metamaterial absorber based on strontium titanate (STO) resonator structure. Opt Commun 2020;462. https://doi.org/10.1016/j.optcom.2020.125265.

[36] Wang Ben-Xin, Wang Gui-Zhen, Wang Ling-Ling. Design of a novel dual-band terahertz metamaterial absorber. Plasmonics 2016;11:523–30. https://doi.org/10.1007/s11468-015-0076-2.

[37] Wang Ben-Xin. Quad-band terahertz metamaterial absorber based on the combining of the dipole and quadrupole resonances of two SRRs. IEEE J Sel Top Quantum Electron 2017;23(4). https://doi.org/10.1109/JSTQE.2016.2547325.

[38] Wang Ben-Xin, He Yuanhao, Lou Pengcheng, Zhu Huaxin. Multi-band terahertz super absorbers based on perforated square-patch metamaterials. Nanoscale Adv 2021;3:455. https://doi.org/10.1039/d0na00903b.

[39] Liu J, Zhu M, Zhang N, Zhang H, Zhou Y, Sun S, et al. Wafer-scale metamaterials for polarization-insensitive and dual-band perfect absorption. Nanoscale 2015;7:18914–7. https://doi.org/10.1039/C5NR05479F.

[40] Mkhitaryan VK, Ghosh DS, Rudé M, Canet-Ferrer J, Maniyara RA, Gopalan KK, et al. Tunable complete optical absorption in multilayer structures including Ge2Sb2Te5 without lithographic patterns. Adv Opt Mater 2017;5(1):1600452. https://doi.org/10.1002/adom.201600452.

[41] Cheng Y, Zou H, Yang J, Mao X, Gong R. Dual and broadband terahertz metamaterial absorber based on a compact resonator structure. Opt Mater Express 2018;8(10). https://doi.org/10.1364/OME.8.003104.

[42] Zhang Y, Cen C, Liang C, Yi Z, Chen X, Li M, et al. Dual-band switchable terahertz metamaterial absorber based on metal nanostructure. Results in Physics. 2019;14(102422). 10.1016/j.rinp.2019.102422.

[43] 45. Jain P, Singh AK, Pandey JK, Bansal S, Gupta N, Singh AK, et al. Ultra-thin and Dual Band Metamaterial Absorber for Terahertz Applications. 6th Edition of International Conference on Wireless Networks & Embedded Systems (WECON). 2018 18951284. 10.1109/WECON.2018.8782070.

[44] Wang B-X, Tang C, Niu Q, He Y, Chen T. Design of narrow discrete distances of dual-/triple-band terahertz metamaterial absorbers. Nanoscale Res Lett 2019;16(64). https://doi.org/10.1186/s11671-019-2876-3.

[45] Mishra Rishi, Panwar Ravi. Investigation of graphene fractal frequency selective surface loaded terahertz absorber. Opt Quant Electron 2020;52:317. https://doi.org/10.1007/s11082-020-02433-2.

[46] Zamzam Pouria, Rezaei Pejman, Khatami Seyed Amin. Quad-band polarization-insensitive metamaterial perfect absorber based on bilayer graphene metasurface. Physica E 2021;128. https://doi.org/10.1016/j.physe.2021.114621. 114621.

[47] Md. Abu Sayeed, Hasan Khaled Rouf. Fabrication and Characterization of Zinc Selenide (ZnSe) Thin Film in Solar Cell Applications. International Conference on Innovations in Science, Engineering and Technology. 2018. 10.1109/ICISET.2018.8745544.

[48] Choudhari Upasana, Jagtap Shweta. Hydrothermally synthesized ZnSe nanoparticles for relative humidity sensing application. J Electron Mater 2020;49:5903–16. https://doi.org/10.1007/s11664-020-08320-6.

[49] 51. Zhenhong Wang, Feng Li, Jia Guo, Chunyang Ma, Yufeng Song, Zhenwu He, Jun Liu, Yupeng Zhang, Delong Li, Han Zhang. Facile Synthesis of 2D Tin Selenide

for Near- and Mid-Infrared Ultrafast Photonics Applications. Advanced optical materials. 2020:(8):6: 1902183. 10.1002/adom.201902183.

[50] Cheng Yongzhi, Gong Rongzhou, Cheng Z. A photo excited broadband switchable metamaterial absorber with polarization-insensitive and wide-angle absorption for terahertz waves. Optical communications 2016;361:41. https://doi.org/10.1016/j.optcom.2015.10.031.

[51] 53. Yong Zhi Cheng, Mu Lin Huang , Hao Ran Chen , Zhen Zhong Guo, Xue Song Mao , Gong RZ. Ultrathin six-band polarization-insensitive perfect metamaterial absorber based on a cross-cave patch resonator for terahertz waves. Materials. 2017;10(6):591. 10.3390/ma10060591.

[52] Chen H-T. Interference theory of metamaterial perfect absorbers. Opt Express 2012;20(7):7165–72. https://doi.org/10.1364/OE.20.007165.